FluidFM-Based Fabrication of Nanopatterns: Promising Surfaces for Platelet Storage Application

Gurunath Apte, Michael Hirtz,* and Thi-Huong Nguyen*

ABSTRACT: Platelets are cell fragments from megakaryocytes devoid of the cell nucleus. They are highly sensitive and easily activated by nonphysiological surfaces. Activated platelets have an intrinsic mechanism to release various proteins that participate in multiple pathways, initiating the platelet activation cascade. Surface induced platelet activation is a challenge encountered during platelet storage, which eventually leads to aggregation of platelets and can thereby result in the degradation of the platelet concentrates. We have previously reported that surface induced platelet activation can be minimized by either modifying their contact surfaces with polymers or introducing nanogroove patterns underneath the platelets. Here, we investigated the response of platelets to various nanotopographical surfaces printed using fluidic force microscopy (FluidFM). We found that the hemispherical array (grid) and hexagonal tile (hive) structures caused a reduction of surface stiffness, which leads to an inhibition of platelet adhesion. Our results reveal that nanopatterns enable the inhibition of platelet activation on surfaces, thus implying that development in nanotexturing of storage bags can extend the lifetime of platelet concentrates.

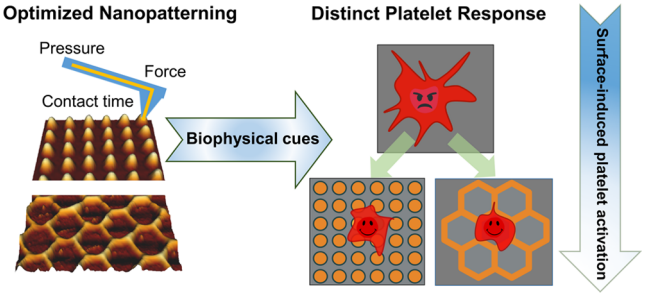

KEYWORDS: *FluidFM, nanopatterning, structured surfaces, surface induced platelet activation, additive surface structuring*

1. INTRODUCTION

Platelets, also known as thrombocytes, are a core component of the human blood coagulation system. Platelets originate as nucleus free cell fragments from megakaryocytes, are about 1.5−3 μm in diameter, and are only less than 1% of the total blood volume.[1−3] Despite this, platelets have an intrinsic mechanism to release various chemokines and cytokines when triggered by an external mechanical or chemical stimulus.[4] Platelets are packed with α granules, dense granules, and lysosomes, consisting of several membrane associated receptor proteins, soluble cargo proteins, cations, bioactive amines, polyphosphates, and pyrophosphates.[5] These granules control the regulated secretion of the soluble agonists, which undergo conformational changes in their structure and contribute to platelet adhesion and activation. In principle, adenosine diphosphate (ADP), thromboxane A2, and thrombin are a few of the platelet activation factors, which participate in multiple pathways that lead to platelet activation.[6,7] They further trigger the activation of other healthy dormant platelets to form a cascading mechanism, which eventually results in the formation of platelet aggregates. Such aggregation is irreversible, thereby resulting in the degradation of the platelets.[8]

Platelet activation by surfaces is a phenomenon that strongly compromises the functionality of platelets when they are stored in vitro, thereby reducing the time for which platelets remain viable for transfusion.[3] Additionally, surface induced platelet activation is of great concern when dealing with blood contacting medical devices and transfusion apparatus. Venous catheters, vascular grafts, stents, and heart valves have previously been associated with thrombotic complications resulting in their failure.[9] Platelet concentrates are in high demand as every day around 1300 L of platelet concentrates are transfused in Germany alone.[10] Undesirable factors such as bacterial or viral contamination[11] and possible health hazards due to the toxic plasticizers pose an additional challenge for a successful transfusion as these factors can induce platelet activation and therefore reduce the lifetime of platelets.[12] Although significant research is carried out to minimize current limitations, surface induced platelet activation remains a rather unaddressed issue.

Surface induced platelet activation can be mitigated mainly by the application of two strategies: chemical modifications and topographical modifications.[3] Implementation of chemical modifications and in particular their transfer into a marketable

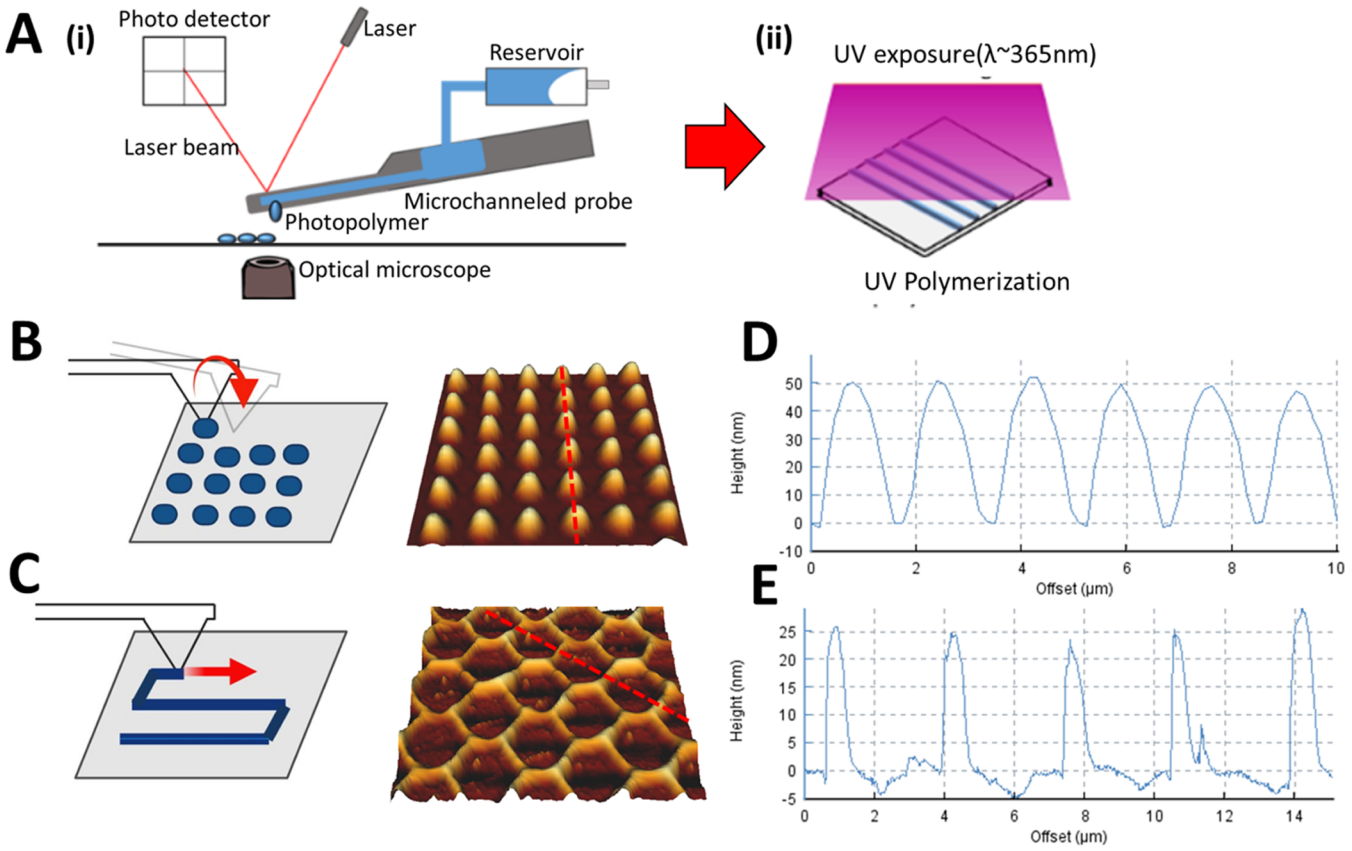

Figure 1. Fabrication of nanostructured surfaces using FluidFM. (A) Schematic showing the working principle of the FluidFM: (i) printing of structures using ink (blue) utilizing a nanopipette and (ii) UV curing to polymerize the printed structures. (B, C) Diagrammatic representation of two AFM modes used for the process of printing: (B) force mapping mode to fabricate hemispherical grid structures and (C) manipulation mode to print the hive pattern enabled by free movement along the x and y axis allowing fabrication of (right) the respective three dimensional (3D) topographs of the printed structures with red dashed lines showing (D, E) line profiles of the printed features.

product are long processes involving many regulatory challenges.[13] However, topographical modifications can be relatively quick to translate into the market as they do not involve the regulatory hassle of introducing new materials.

It is well known that cells have varied responses of their cellular processes toward topographic modifications.[14] Recent studies with topographical modifications for platelet research by different groups have shown that topography does influence the adhesion and activation trends in platelets.[15−17] Unlike most mammalian cells (with the size of several tens of micrometers) that can be influenced by the underneath surface constructed with multiple microstructures, platelets are much smaller (only 1.5−3.5 μm), and therefore, they only respond to nanostructured surfaces. Nanostructures have been shown to modulate the behavior of even much larger cells. Lenhert et al. have shown the alignment of osteoblasts and germinating fungal spores on nanostructured surfaces with a groove depth down to 100 nm.[18] Emmert et al. recently showed that nanoporous glass with a mean pore size of around 80 nm may be considered as macroscopically flat but serves in modulating the gene expression and thereby influences cellular processes in primary human mesenchymal stem cells, which are much larger than platelets.[19] Wang et al. engineered nanogratings and pillars to investigate the spreading and organization of focal adhesions in human lung fibroblast cells.[20] They found that the discrete topography of nanopillars tended to disrupt the formation and growth of focal adhesions. In the case of platelets, where most of the work so far has been done at the microscale,[21−24] several nanostructured surfaces[25] including nanoparticles[26] and groove structures[17] have also been investigated. In connection with the impact of nanostructures on platelets, we have previously seen significant inhibition of platelet activation by changing the interspacing among nanogrooves.[17] In particular, the non coated gold/pattern with a height of around 100 nm caused an obvious change in the shape of platelets in a different way as compared with flat surfaces or patterns of higher height (around 200 nm). A significant change in the platelet morphology was still obtained when the groove heights were reduced to around 60 nm after the laminin coating.

The mechanism of how platelets take cues about substrate stiffness and switch their activation response has been previously understood as Qui et al. observed the ability of platelets to mechanosense surfaces with varied stiffness and that they undergo cytoskeletal reorganization on harder surfaces.[27] While significant research has been done to establish the theory of how substrate stiffness dictates platelet adhesion, activation, and spreading,[27−29] the notion of tuning the substrate stiffness to in turn mediate these platelet processes remains unexplored. Generally, materials to con struct the discussed nanostructures were metals and further coated with polymers or proteins to adjust the surface properties. Such materials tend to have low biocompatible properties as metal can directly affect platelets, while the coating molecules can be released into the platelet storage buffer and alter its composition. Therefore, a robust method

based on stable nanostructures fabricated on a material with excellent platelet compatibility is highly desired.

Here, we fabricated hemispherical grid pattern and hexagonal tile nanostructures using atomic force microscopy (AFM) based fluidic force microscopy (FluidFM)[30] and investigated the response of platelets on the fabricated structures. FluidFM has shown to be a versatile method for generating functional and topographical features from synthetic[31,32] and biological materials.[33] To print the structures, the force mapping mode was used to produce a hemispherical grid pattern, while the manipulation mode was used to print hexagonal tiles (honeycomb) using a commercial hybrid acrylate based ultraviolet (UV) curable Loctite AA3491 (Henkel). The FluidFM parameters were optimized to dispense the right volume of ink to print the structures reproducibly on the glass. The topography of structures was confirmed using AFM and scanning electron microscopy (SEM) imaging. The effect of the topography was then assessed by quantifying the adhesion and spreading of human platelets on the fabricated surfaces. Nanoindentation measure ments were carried out to measure the stiffness of the printed structures. Hemispherical features and honeycomb structures caused a reduction of surface stiffness, leading to inhibition of platelet adhesion. Our study shows that surface induced platelet activation can be effectively inhibited by introducing nanostructures underneath platelets, which can contribute to the development of platelet storage bags and other medical applications.

2. METHODS

2.1. FluidFM-Based Printing. The structures were fabricated with the help of a Nanowizard 4 setup (JPK, Berlin, Germany) with a FluidFM addon (Cytosurge, Opfikon, Switzerland), positioned under an acoustic hood, and mounted on an active vibration isolation system (Micro 40, Halcyconics, Germany) to minimize the effects of surrounding vibrations. An inverted microscope (Axio Observer Zeiss, Jena, Germany) is used to observe the cantilever and move it to the desired location (Figure 1A).

Evaluation and optimization of FluidFM parameters for printing: All the parameters were systematically optimized by varying only one parameter at a time to evaluate its impact during the printing process. The setpoint and pressure parameters were optimized for both force mapping and manipulation printing modes. In the case of printing in force mapping mode, the effect of contact time was evaluated whereas for manipulation mode the effect of writing velocities was assessed.

2.1.1. Printing in the Force Mapping Mode. AFM in the force mapping mode was used to print the array of hemispherical dots on round glass coverslips (Plano GmbH, Wetzlar, Germany) of 24 mm, which were precleaned with 80% ethanol and subjected to 30 min of sonication. The reservoir of the microchannel cantilever was filled with ink (Loctite AA3491, Henkel, Germany), consisting of a blend of various methacrylate esters, which polymerize upon exposure to UV. The Loctite AA3491 is composed of monomers from isobornyl acrylate, 2 hydroxyethyl methacrylate, acrylic acid, and hydroxypropyl acrylate.[34] A nanopipette with an aperture of 300 nm and a nominal spring constant of 2 N/m (Cytosurge, Opfikon, Switzerland) was calibrated before each printing cycle by the contact free thermal noise method before being approached to the surface with a constant pressure of 150 mbar and a setpoint of 10 nN. To investigate the effect of contact time on printing quality, the nanopipette was kept in contact with the surface up to 20s. The optimal contact time was then determined at 2.5 s and used in the later experiments. The nanopipette was scanned over an area of 50 × 50 μm^2 with a pixel size of 30 × 30, leading to an array of 900 hemispherical features. After printing, the samples were exposed to a UV lamp at ∼365 nm for 5 min for curing.

2.1.2. Printing in the Manipulation Mode. AFM in the manipulation mode was used to print the hexagonal tile structure on a glass coverslip. The structure was predesigned using graphic software Inkscape (version 0.17), which allows the user to create the desired pattern in an exportable scalable vector graphic file (svg). This file was then imported to AFM control software JPK Nanowizard4. The printing was carried out in an area of 50 × 50 μm^2. To investigate the effect of applied preasure, setpoint, and writing speed on the printing quality, these parameters were varied up to 700 mbar, 20 nN, and 2 μm/s, respectively. The optimal parameters were determined at 150 mbar pressure, 10 nN setpoint, and 1 μm/s speed that were then used for later experiments. After printing, the samples were cured as described above.

2.2. Spin Coating. To generate a uniform layer of polymer on the surface, 10 μL of ink was dropped on the cleaned glass coverslips and spun with a WS 500B 400BZ 6NPP Lite spin coater (Laurell technologies corporation, Pennsylvania) at 6000 rpm for 1 min. After coating, the samples were exposed to UV for curing as described above.

2.3. Characterization of the Topography Using Atomic Force Microscopy. The topographical scans were acquired using AFM in the force modulation mode. All samples were imaged at a line rate of 0.3 Hz and a resolution of 512 × 512 pixels. A cantilever from Mikromasch (HQ: CSC38/tipless/No AI) with a nominal spring constant of 0.09 N/m was used. The scan size of 80 × 80 μm^2 was used to completely image the 50 × 50 μm^2 printed patterns. The line profiles of the features were obtained by selecting the image cross section option to compute the size of each printed feature using JPK software. The base diameter, interspacing, and height of 10 hemispherical features and height and diagonal spacing for 10 hive features were measured to calculate the mean and standard deviation. The roughness parameters were calculated over an area of 15 × 15 μm^2 using JPKSPM data analysis software to compute the average (Ra) and RMS (Rq) roughness values over all the surfaces. For imaging of platelets on surfaces with AFM, the platelets were fixed with paraformaldehyde (PFA), rinsed with phosphate buffer solution (PBS), and imaged in the force modulation mode in PBS using the same above mentioned cantilever type at a scan rate of 1 Hz. Image processing was done in JPK Nanowizard4 software.

2.4. Nanoindentation. The mechanical properties of the fabricated nanopatterns, spin coated polymer, and glass were measured by nanoindentation with AFM. Here, a cantilever with a gold bead with a diameter of 3 μm (CP CONT AU A, Nanoandmore GmbH, Germany) was used to indent the samples. For each sample, 2500 pairs of force vs displacement curves were obtained over the surface from a 20 × 20 μm^2 area by subdividing the area into equal sized pixels and acquiring one pair of curves from the center of each pixel. The tip velocities and the z length for these measurements were 3 μm/s and 3 μm, respectively. The measurements for all the samples, except the spin coated sample, were done in the air with an applied force of 1000 pN. The measurement on spin coated polymer could not be achieved under the same conditions in air, due to the strong adhesive force between the cantilever tip and the surface. This results in the tip being held on the sample after indentation, not allowing the cantilever to return to the rest position. Therefore, to obtain at least some comparison, the measurement for the bulk polymer was done in liquids, where the full indentation cycle could be performed (Figure S1). The calibrated spring constant of the cantilever for processing the force curves was 0.03 N/m in air. The stiffness of each sample was evaluated by fitting the corresponding extend/approach curve to the Hertz model.[35] The tip geometry during the calculations was considered as a sphere with a tip diameter of 3 μm. The Hertz model is given by the following formula

$$F = \frac{4E\sqrt{R}\delta^{3/2}}{3(1-\nu^2)} \quad (1)$$

where F is the applied force, δ is the indentation depth, R is the radius of the spherical tip, ν is the Poisson ratio, and E is Young's Modulus.[35] Data analysis was performed using Sigmaplot.

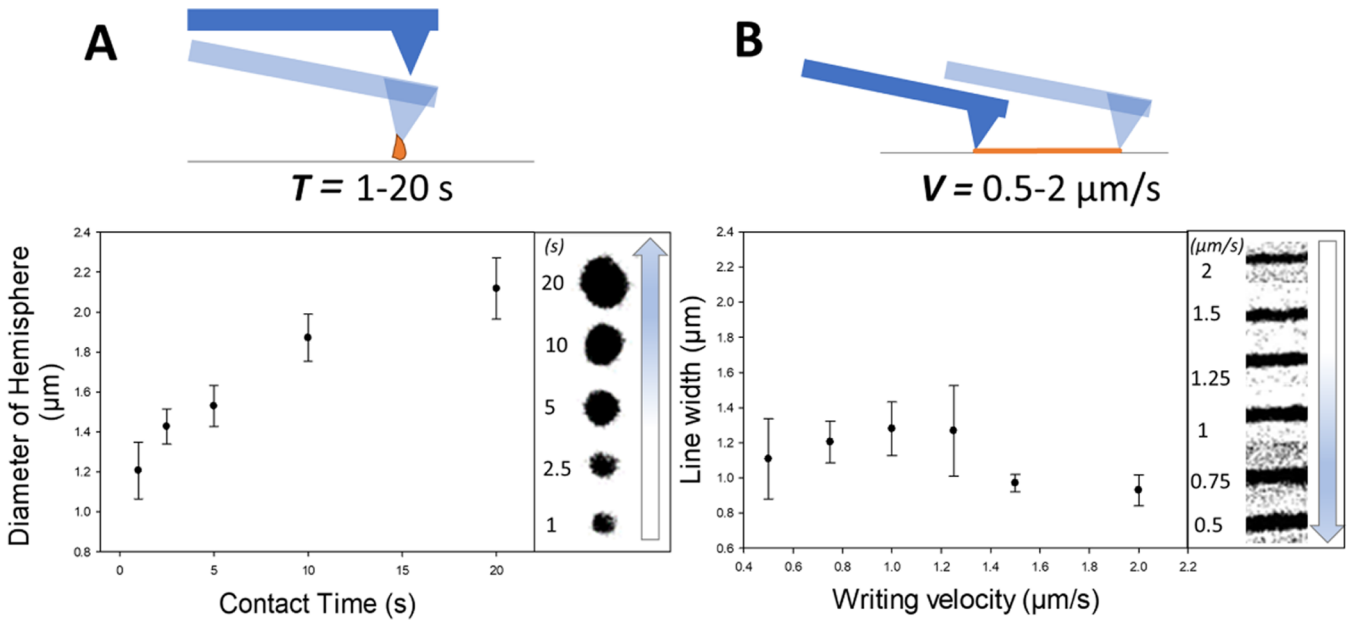

Figure 2. Optimization of printing parameters. Influence of contact time and writing speed as a printing parameter on the extruded volume of ink and size of the printed structure in (A) force mapping mode to print dots and (B) manipulation mode to print lines. The SEM images (on the right of each graph) of dots and lines are shown for the respective points on the *x* axis.

2.5. Isolation of Platelets. Blood from healthy human donors who were drug free within the previous 2 weeks was collected into a tube of acid citrate dextrose ACD A 1.5 mL (BD Vacutainer, Berlin, Germany). Before centrifugation, the blood tube was sealed with parafilm, inclined at an angle of 45°, and rested at room temperature for 15 min. Platelet rich plasma (PRP) was first obtained from the blood by centrifugation at 120*g* for 20 min at room temperature. Platelets were further isolated from PRP in the presence of 15% ACD A (Fresenius Kabi, Germany) and 2.5 U/mL apyrase (grade IV SIGMA, Munich, Germany) by centrifuging at 650*g* for 7 min. The platelet pellet was resuspended in 1 mL of suspension buffer at pH 6.3 composed of 137 mM NaCl, 2.7 mM KCl, 11.9 mM $NaHCO_3$, 0.4 mM Na_2HPO_4, and 2.5 U/mL hirudin. A total of 4 mL of additional suspension buffer was added to the platelets and incubated for 15 min at 37 °C. The suspension was then recentrifuged at 650*g* for 7 min. Platelet pellets were once again resuspended in 2 mL of suspension buffer, followed by platelet counting performed using a blood counter (pocH 100i, SYMEX, Germany). The platelet concentrations were further adjusted in a suspension buffer according to the requirement.

2.6. Platelet Adhesion and Spreading. Platelets at a concentration of 30,000/μL were added to the samples and incubated for 1 h. Unbound platelets were removed by rinsing with phosphate buffered saline (PBS), and the platelets were fixed using 4% paraformaldehyde (PFA) for 30 min. Confocal reflection microscopy was used to count the number of platelets adherent to the samples. Four samples for each condition from three independent donors, with an area of 50 × 50 μm^2, were quantified to obtain statistics for adhesion and spreading of the platelets. To quantify the spreading of platelets on the surface, the platelets after fixation were stained for 1 h with anti CD42a FITC antibodies (Dianova GmbH, Hamburg, Germany) with a final concentration of 0.1 μg/mL of platelet solution. The unbound dye was then rinsed off the sample by washing with PBS twice. After that, samples were incubated with permeable buffer for 10 min, followed by the addition of phalloidin DY590 (Mobitec GmbH, Göttingen, Germany) (1:20 dilution) for 45 min of incubation at RT (23 °C) in the dark. Samples were examined using a Zeiss LSM710 confocal laser scanning microscope (Carl Zeiss, Gottingen, Germany) at RT in the dark. The blue fluorescent signal was acquired using the excitation/emission wavelength λ = 488/520 nm, and the red fluorescent signal was acquired using the excitation/emission wavelength λ = 580/599 nm, respectively, using a 63× objective. Images were also taken with a T80/R20 beam splitter to visualize the patterns by confocal reflection microscopy.[36] ImageJ software was used to further process the images and to quantify the adhesion and spread of the platelets on each sample.[37,38] Images from both channels (blue and red) were imported, followed by adjustments in contrast and brightness. Images were converted to a stack and cropped to select the area of 50 × 50 μm^2 before being converted back to images from individual channels. The images were then analyzed using the thresholding tool from ImageJ to measure the overall platelet spreading, followed by the application of the particle analysis tool to quantify the number of platelets. To visualize the nanostructures, confocal reflection microscopy images were merged with the individual images from both channels before being assigned pseudocolors by applying the Look up table (LUT) tool.

2.7. Scanning Electron Microscopy (SEM). The samples with printed features for parameter optimization were sputtered with gold and imaged with an Evo LS10 SEM (Carl Zeiss AG, Jena, Germany). The images were then processed to set the optimum brightness and contrast with ImageJ. Images were processed using the tool and converted to binary images for further evaluation. A measurement tool was used to compute the diameter of hemispherical features printed in the force mapping mode and the width of the lines printed in the manipulation mode.

2.8. Water Contact Angle. The static contact angle for the glass and spin coated samples was measured using an OCA 15+ system (Data Physics Instruments GmbH, Filderstadt, Germany) with the sessile drop method. The dosing volume was set to 3 μL, and the ellipse fitting method was used to compute the contact angle with the help of OCA15+ software.

2.9. Single-Platelet Force Spectroscopy (SPFS). The single platelet force spectroscopy (SPFS) measurements were performed with AFM (JPK, Berlin, Germany) assembled with a FluidFM (Cytosurge, Glattbrugg, Switzerland) add on device. The micro channel cantilever with an aperture of 2 μm and nominal spring constant of 2 N/m (Cytosurge, Glattbrugg, Switzerland) was approached toward platelets by applying a pressure of −800 mbar. The largest visible platelets (as they are expected to be larger than the cantilever aperture) were targeted to avoid sucking the platelet into the microchannel cantilever. Once the platelet was picked, the pressure was reduced to −200 mbar and the cantilever was retracted. Subsequently, force mapping was performed to generate force−

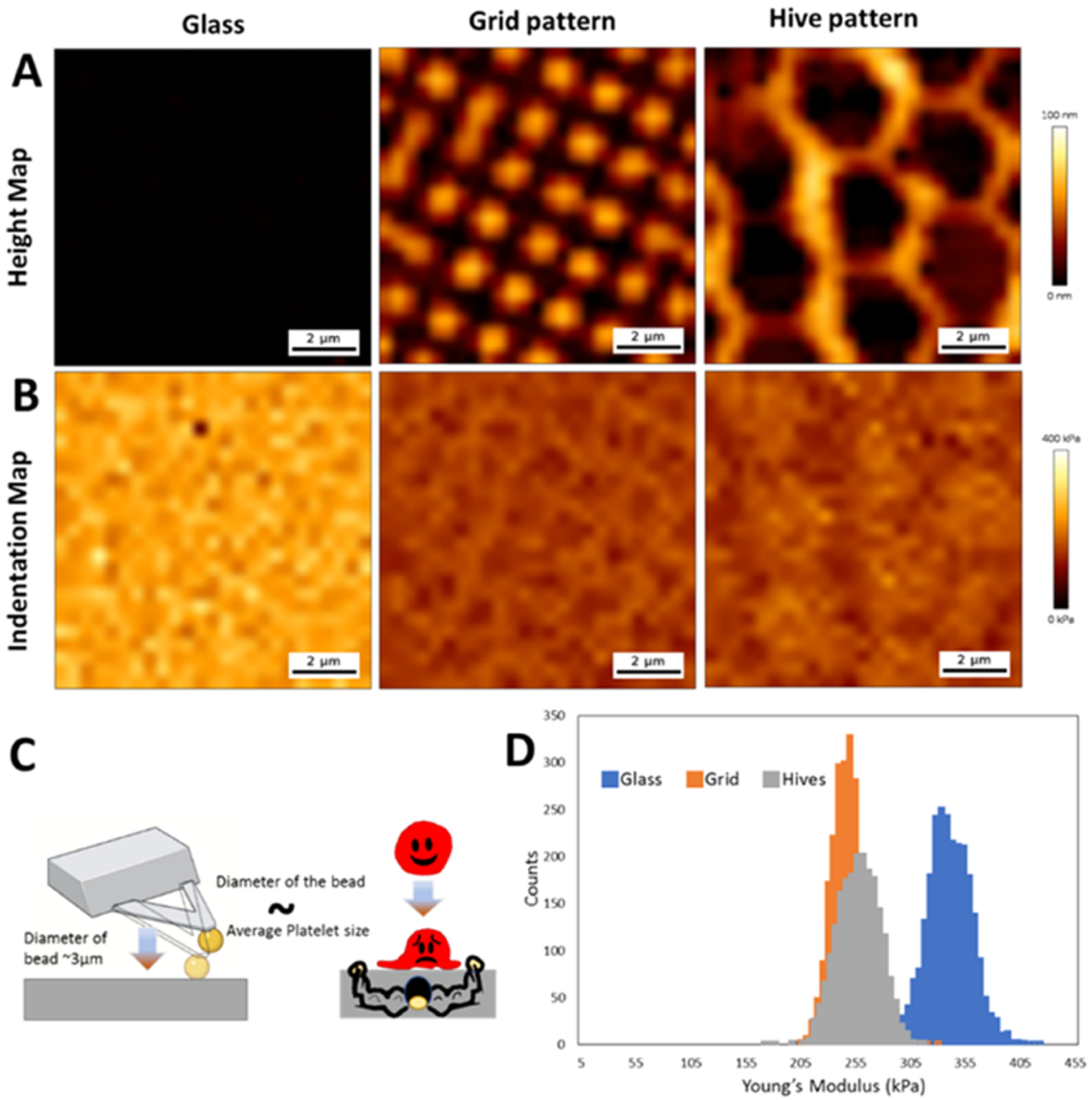

Figure 3. Determination of the stiffness of the patterns. (A) Height maps of bare glass, grid and hive patterns along with their respective (B) indentation maps. (C) Schematic representation of nanoindentation carried out using a cantilever with a bead to comprehend the stiffness experienced by a platelet on different surfaces and (D) distribution of E modulus values on the different surfaces.

displacement ($F-D$) curves over glass, fabricated nanopatterns, and spin coated polymer surfaces. Independent platelets were picked up and measured on each surface. An area of 20 × 20 μm^2 was subdivided into 20 × 20 equal sized pixels. The force−distance curves over all samples were recorded at a setpoint of 5 nN, z length of 5 μm, and pulling speed of 2 μm/s. The force curves were processed in JPKSPM data processing software, and the adhesion forces were calculated. The values were presented in the form of scatter and box plots using Sigmaplot 14.0 (Sysstat Software GmbH, Erkrath, Germany).

3. RESULTS

3.1. Topography of Nanopatterns. The schematic in Figure 1A outlines the FluidFM based printing process, followed by a step involving UV exposure to stabilize the fabricated structures (Figure 1A).

Using different printing modes, we fabricated the hemi spherical grid and the hexagonal hive pattern as shown in the cartoons (left, Figure 1B,C). To visualize the fabricated patterns, samples were imaged using AFM in the force modulation mode, and the diameters and the heights of the structured surfaces were measured. Figure 1B,C (right) shows the 3D topographs of the grids and hives with a red dashed line marking the position where the line profiles presented in Figure 1D,E are extracted from. The line profiles of glass and spin coated polymer surfaces show them as macroscopically smooth surfaces in comparison to the nanopatterns (Figure S2). The average diameter for the hemispheres in the produced grids is 1000 ± 80 nm, height is 48.0 ± 1.4 nm, and interspacing between two features is 672 ± 54 nm. In the case of the hive patterns, the average internal diagonal distance for the hexagons is 3.1 ± 0.1 μm, while the height of the features is 26.4 ± 3.3 nm.

3.2. Optimization of Printing Parameters. In FluidFM, parameters such as setpoint, pressure, and contact time govern the quality of the printing nanostructures. To understand the influence of these parameters on the printing process and identify the protocol that allows reproducible fabrication of the desired structures, we fabricated the structures in a wide range of setpoints, pressures, and contact times, i.e., up to 20 nN, 700 mbar, and 20 s, respectively. The parameters such as z length

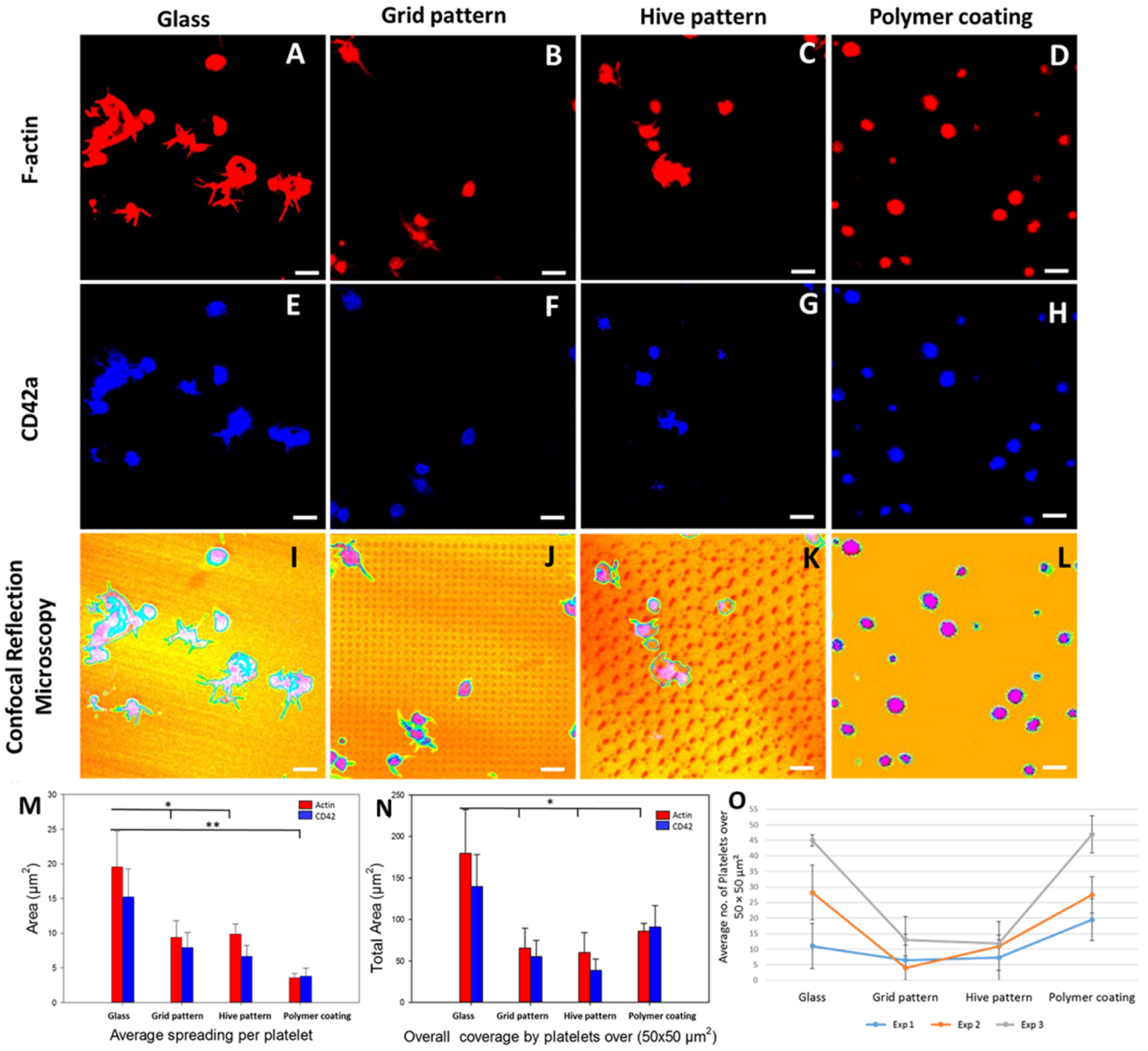

Figure 4. Platelets response on nanostructured surfaces obtained by confocal reflection microscopy. (A–D) Actin fibers of platelet were stained by DY590 phalloidin (red) and (E–H) surface expressed protein CD42a was stained by anti CD42a FITC conjugated antibody (blue). For each sample, images were post processed and merged with the images taken by setting the filter T80/R20 to get a clear visualization of platelets together with the unstained patterns (I–L). Quantification of the fluorescence signal from both stains to obtain the (M) average spreading area per platelet and (N) total area covered by platelets on a defined area of 50 × 50 μm^2. (O) Graph representing the number of adhered platelets obtained from three independent experiments with platelets from three independent donors. Scale bars equal 5 μm for all images. Statistically significant difference determined by one way ANOVA using the Bonferroni t test **($P < 0.05$), *($P < 0.001$). Scale bars equal 5 μm for all images.

and the extended speed were kept correspondingly constant throughout at 5 μm and 2.5 μm/s.

The effect of printing parameters was obtained by comparing the change in the size of the printed features. In the case of the force mapping mode, 10 hemispherical dots were printed for each measurement condition before being cured and gold sputtered, following which the sample was imaged by SEM. The SEM images were converted to a binary image for better visualization using the tool from ImageJ, following which the diameter of the dots was measured (Figure 2). Similarly, for the manipulation mode, a 30 μm line was printed, following which the width was averaged at five different points to obtain the mean value.

In the event of studying the impact of contact time (Figure 2A), the increase in the diameter of the hemisphere with increasing time was evident with the diameter of the hemispheres, almost doubling from 1 to 20 s. In the case of writing velocity, it was observed that the width of the printed line decreased after 1.0 μm/s (Figure 2B). Interestingly, in both modes of printing, the time for which the pipette is in contact with the surface is the factor that seemed to influence the printing process the most. Thus, to summarize, a slower speed of writing or higher contact time resulted in thicker features.

In the case of variation of other parameters in the force mapping mode, it was seen that the setpoint (Figure S3A) has

a negligible impact over a large range since no clear trend was seen over the range of 2−20 nN. In the case of pressure (Figure S3B), the features showed no change in diameter till a positive pressure reached >400 mbar, in which the diameter increased.

Regarding the parameters in the manipulation mode, variation of the setpoint (Figure S3C) and pressure (Figure S3D) showed no visible trends in particular as can be witnessed by the high deviation bars overlapping over each other. Together, the setpoint of 10 nN and pressures in the range of 50−150 mbar are the most suitable parameters for printing nanostructures.

3.3. Stiffness of the Printed Nanostructures. As surface properties play an important role in controlling surface induced platelet activation, we next characterized the stiffness of the structured samples. Nanoindentation experiments were carried out using a colloidal probe of 3 μm diameter. Upon indentation of the probe on the structured surfaces, a force−distance ($F-D$) curve is recorded, from which the stiffness of the surface can be analyzed. Figure 3A shows the topographic height map of the surfaces, and Figure 3B indicates the map of Young's modulus values calculated by fitting the $F-D$ curves by the Hertz model. The rationale to use a colloidal probe with a comparable diameter of the platelet was to understand the stiffness sensed by a similar sized object (Figure 3C). The histograms plotted in Figure 3D display the distribution of the stiffness sensed by the probe. The grid pattern shows a mean value of 244.9 ± 15.0 kPa, while the hive pattern median is 253.3 ± 18.9 kPa. Both printed structures overall appear to be softer on the probed length scale when compared to the glass with a median value of 338.5 ± 21.9 kPa.

3.4. Response of Platelets on Structured Surfaces. To track how the platelets respond to the fabricated structures, we seeded platelets on the samples for 1 h and counted the number of platelets adhered to the structured area or nonstructured areas of the same size. The number of platelets adhered to the spin coated polymer was highest followed by that of bare glass, whereas the structured surfaces with grid and hive patterns showed lower platelet adhesion (Figure 4).

To further understand the platelet adhesion on the patterns, we characterized the cellular adhesion and spreading properties using different platelet staining materials. Phalloidin, the first dye, stained the actin filaments in the platelets, providing detailed information about the filopodial and lamellipodial outgrowths developed by the activated platelets (Figure 4A−D). The second dye is FITC conjugated anti CD42a antibody, which acts as an identifier for platelets, thereby confirming their presence. The micrographs (Figure 4I−L) provide merged images obtained by confocal reflection microscopy together with the fluorescence images of the phalloidin and FITC signals. In this mode, the printed structures underneath the platelets, which are not seen the in fluorescence images, can be discerned. The graph in Figure 4M shows the average area of platelets in the two stainings, the difference of which can be interpreted as the spreading of activated platelets. On the spin coated polymer, no obvious spreading was observed (signal obtained by the actin stain was equal to that from CD42), while the patterned samples showed increased spreading, but it was highest on glass. The comparison of the overall surface area covered by platelets (Figure 4N) suggested that there is a significant difference between glass and other samples; however, no significant difference was observed between the spin coated polymer and grid and hive patterned samples. In the comparison of the intensity of the signal from both dyes, it was seen that among the fabricated nanostructures, the grid patterns were more restrictive toward platelet spreading. In the case of adhesion experiments (Figure 4O), the trend showed higher platelet adhesion on glass and the polymer coated surfaces, whereas the number of platelets on the grid and hive patterned surfaces were relatively lower, thus indicating that the structured surfaces impeded adhesion of the platelets. Consistently, when single platelets were picked up with FluidFM cantilevers and the interaction force between platelets and surfaces was measured, we found the highest deadhesion forces when platelets interacted with the polymer coating, followed by nanostructured surfaces, and the lowest on bare glass (Figure S4).

3.5. Discussion. In this study, we demonstrated that FluidFM can be used in different modes to fabricate polymer nanostructures for platelet adhesion studies. The geometry and size of the features can be varied by tuning the physical printing parameters. We established the optimum parameters to fabricate and successfully reproduce stable hemispherical grid patterns and hexagonal hive nanostructures. Both of the patterned surfaces inhibit platelet adhesion better as compared to their control counterparts of either the bare glass or spin coated polymer. The grid patterned structures were found to inhibit the platelet adhesion slightly more (although not significantly) as compared to the hive patterns. The patterns also showed a considerable decrease not only in the development of platelet lamellipodia but also in suppressing filopodia or the outer protrusions, as compared to the plain glass surface.

Our findings corroborate previous studies revealing platelet mechanosensing of the underlying surface stiffness, undergoing a reorganization of the cytoskeleton, higher adhesion, and more spreading on harder surfaces because of the elevated α granule secretion and αIIbβ3 integrin activation.[27] Such procoagulant activities leading to platelet activation are a response to the mechanical forces sensed at the adhesive junctions between the platelet and the platelet−surface interface.[39] Thus, along with the receptor ligand activation, which is usually responsible for the platelet activation and aggregation, the biophysical interaction between the platelet and its contact surface also dictates the fate of the platelet activation cascade. In our study, we observe that there is a significant variation in the overall stiffness of the bare glass as compared to the spin coated sample and also a considerable difference between bare glass and the fabricated nanopatterns. This trend in stiffness also translates in the way how platelet spreading on different surfaces takes place (Figure 4M). Although our observations on platelet spreading concur with the above mentioned theory, our findings in the case of the spin coated polymer however are seemingly in contrast to the substrate stiffness−platelet adhesion analogy. However, this first sight counterintuitive finding may be attributed to the higher hydrophobicity of the polymer coated surface (contact angle of 77.9 ± 5.0°) as compared to bare glass (contact angle of 43.0 ± 1.9°). The higher hydrophobicity of the surface facilitates the adsorption of proteins expelled from the platelets, thereby helping the initial docking of platelets to the surface. Then, due to the low stiffness of the spin coated polymer substrate, spreading remains at a minimum. The spin coated polymer surface showed the highest adhesion of platelets. As platelet adhesion is the first step that leads to platelet activation,[40,41] the spin coated surface is not suitable

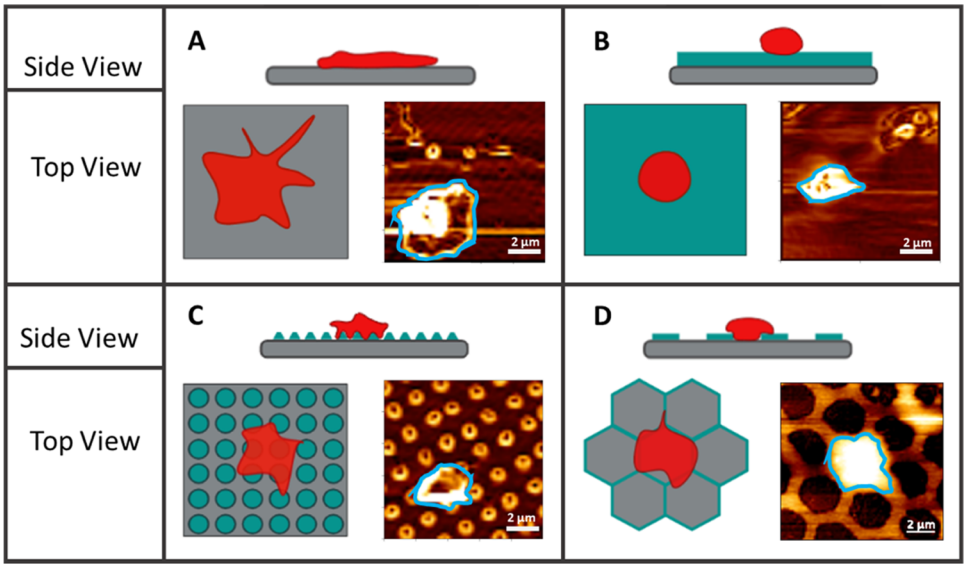

Figure 5. Changes in the platelet morphology on nanopatterns. Models showing the morphology of platelets on surfaces from the side and top view accompanied by AFM images of the platelets marked with a blue boundary from (A) glass, (B) polymer coating, (C) grid pattern, and (D) hive pattern.

for platelet storage. The adhering platelet counts for the two fabricated nanopatterns showed that the number of platelets on the grid pattern was only slightly lower as compared to that on the hive pattern. The difference in the spreading areas represented in Figure 4M,N also does not point out any significant difference. However, on careful analysis of the discrepancy in the stained area from actin and CD42a dye, we obtain some insights into the behavior of platelets on the two different nanostructured samples. The expressed actin activity in the grid pattern is 1.19×, whereas in hives, it is 1.55× in comparison to the CD42a. This higher shift in the ratios of F actin to CD42a staining for the hive patterns indicates the wider spread of actin filaments, thereby suggesting a higher degree of platelet activation.

Although confocal microscopy allowed for the quantification of platelet spreading trends on different surfaces, the strength of the interactions between platelets and surfaces would be an additional interesting property for complete characterization. The strong forces measured on the polymer coating explain the high density of adhering platelets seen on this surface. Surprisingly, the glass showed the lowest deadhesion forces (Figure S4), but a high density of adhesion and strong activation of platelets were seen from confocal micrographs (Figure 4). Here, probably, the high stiffness of the glass played a role as platelets are known to be activated by hard surfaces,[27] and sufficient long seeding time also caused platelet activation on bare glass. Furthermore, platelet adhesion on surfaces is influenced by the charge and surface energy.[41] The weak adhesion force on glass could be due to the electrostatic repulsion between the negatively charged platelet membrane, which is composed of anionic glycocalyx, and the negatively charged glass surface. Furthermore, hydrophilicity might also play a role as the glass surface exhibits higher hydrophilicity than that of the polymer coating. Unlike the hydrophobic surfaces that facilitate protein binding, hydrophilic surfaces are known to inhibit protein binding due to the presence of water molecules, which are difficult to be displaced by the adsorbing proteins.[41,42] Thus, the platelets might experience less adhesive forces, and this may have contributed to the reduction of the overall deadhesion force measured within the short contact time of platelets to the glass surface. Interactions of platelets with nanostructures showed higher deadhesion forces than on glass but much lower than on the polymer coating. This reflects the combined behavior of both polymers (the patterns) and glass (the interface within the patterns). Overall, the results make the low density of platelets adhered on the printed nanostructures plausible, keeping in mind possible the synergistic effects of adhesion and stiffness.

The spreading of platelets is not only attributed to the stiffness, chemistry, and wetting properties of the surface but also to the surface roughness. Generally, surface roughness is critical in modulating cellular processes.[43] The roughness parameters Ra and Rq show that the overall roughness was found to be higher for the nanopatterned surfaces as compared to the unpatterned controls (Table S1). We have previously reviewed numerous studies carried out exploring the effect of topologies on the inhibition of platelet adhesion.[3] In some cases, topography suppressed the protein adsorption, thereby restricting the platelet adhesion,[15,44] while for others, it induced a minimal contact area between the platelet and surface.[17] Nanotopology induces an increase in the roughness of the overall surface (Table S1) and can therefore dictate the process of platelet spreading.

Based on the results obtained, we propose a schematic depicting the response of platelets on the different surfaces (Figure 5). The schematics and the corresponding AFM images show a side view and top view of the platelets on each surface, providing insights as to how the platelets take topographical cues from the surface and restrain their activation process. Grid and hive patterns are two examples of continuous and discontinuous topographies, respectively. We hypothesize that the hemispherical structures in the grid form can mimic the physiological endothelial cell lining, thereby providing biophysical cues, which platelets can perceive and therefore discourage the process of platelet activation, whereas in the case of hive patterns, the perimeter of the hexagonal features will assist in restricting the probing and extension mechanisms exhibited by the filopodial out

growths. The "platelet like shape" of the hexagon is likely a favorable structure for platelets. The symmetrical boundary of the hexagonal feature could probably generate a homogeneous environment including forces and stiffness that act equally at all contacting parts of a platelet body.

As platelets activate immediately when contacting with nonphysiological surfaces, inhibition of surface induced platelet on artificial surfaces including platelet storage bags and implants is highly desired to overcome the limitations in many biomedical applications. We proved that nanopatterns fabricated using the UV curable Loctite polymer allowed us to strongly reduce surface induced platelet adhesion and activation.

4. LIMITATIONS AND FUTURE PERSPECTIVES

While already, nanostructures have a significant impact on even much larger biological entities, it would be interesting to follow up on the impact of the same structures as explored here with larger heights. This cannot be readily achieved with our present setup due to technical reasons, although in general, FluidFM with polymer inks is capable of layer by layer 3D printing.[31] Even though our study focused on the modulation of platelet adhesion and activation by surface topography, other factors such as roughness and wetting behavior also play a crucial role in the process of platelet adhesion. Recently, we observed that the height of structures can be slightly enlarged by modifying the wetting properties of the substrate, but the change in substrate hydrophilicity would also impact platelet adhesion on its own.[45] While roughness is readily accessible by AFM measurements of the patterns, the wetting properties are much harder to access as of the limited patterning area of only $50 \times 50\ \mu m^2$. However, by providing the contact angles for the accessible substrates (glass and spin coated polymer), a general range of expected contact angles on the nanopatterns can be estimated. Lastly, several factors such as bacterial contamination, storage lesions, pH, temperature, and storage medium pose great challenges in the development of ideal platelet storage bags.[3] The substrate material also plays an important role as it governs the gas permeability[46] and controls the adsorption of various proteins,[9] which can dictate the activation process. Furthermore, the presence of endogenous or exogenous antioxidants and the formation of reactive oxygen and nitrogen species may alter platelet function[47] and lead to platelet aggregate formation; therefore, integration of antioxidants into nanostructures may allow us to create an antioxidative capability of platelets within a bag. While it would be interesting to combine a change in materials with the same patterns, the scope of our current work was focused on the patterns as such, therefore limiting ourselves to only one polymer. In the future, already optimized and ideally regulatory approved materials could be studied for the potential to further improve their platelet storage properties using nanostructures.

Although FluidFM can be readily used to determine the strength of the interactions between a variety of cells and surfaces,[48] this approach requires much more effort to extend to platelet measurements. Single platelet force spectroscopy (SPFS) using FluidFM to directly obtain the adhesion force between single platelets and surfaces is still challenging as the high negative pressure to pick platelets can cause damage to the platelet membrane and may even lead to aspiration of platelets, thus blocking the internal microchannel. Furthermore, the strong adhesion of platelets to the microchannel cantilever occasionally results in blocking of the cantilever aperture. Thus, SPFS using FluidFM requires future refinement, especially in cantilever functionalization to minimize platelet adhesion, spreading, and activation and identification of minimal applied pressure to platelets to reduce platelet damage. In summary, there is still a vast knowledge gap to be addressed for solving the problem of surface induced platelet activation. Additionally, factors such as aspect ratio, interspacing, geometry, and density of the topography should be further considered and optimized to realize an ideal nanostructured surface. For future work, we will investigate the behavior of platelets on nanostructures fabricated with modified inks to integrate blood compatible and platelet repelling chemical moieties into the structures.

5. CONCLUSIONS

We conclude that the easy to use, direct write patterning technique by FluidFM in assistance with the AFM offers cost effectiveness and a reliable solution to fabricate nanopatterns of different geometries in a reproducible way for cell study applications, as exemplified here for platelet activation. We studied the behavior of human platelets on patterned (grid and hive patterns) and nonpatterned surfaces (glass and spin coated polymer). The nanotopography and substrate stiffness play a crucial role in governing the platelet behavior. First and foremost, the results indicated that the fabricated nanostructures were able to curb platelet adhesion and control their spreading. The ability of the nanostructures to restrain the inherent ability of platelets to undergo activation following the primary steps of platelet adhesion and spreading proposes them as a potential contender in the development of nanotextured storage bags for platelets. Prototyping structure candidates by FluidFM patterning for platelet activation studies can help to identify promising geometries that could then be transferred into mass production compatible techniques such as roll to roll imprinting or similar pattern replication approaches.

■ ASSOCIATED CONTENT

● Supporting Information

The Supporting Information is available free of charge at https://pubs.acs.org/doi/10.1021/acsami.2c03459.

> Indentation of the polymer coated surface; line profiles for glass and spin coated polymer; optimization of printing parameters; single platelet force spectroscopy, and roughness parameters (PDF)

■ AUTHOR INFORMATION

Corresponding Authors

Michael Hirtz − *Institute of Nanotechnology (INT) and Karlsruhe Nano Micro Facility (KNMFi), Karlsruhe Institute of Technology, 76131 Karlsruhe, Germany;* orcid.org/0000 0002 2647 5317; Email: michael.hirtz@kit.edu

Thi Huong Nguyen − *Institute for Bioprocessing and Analytical Measurement Techniques (iba), 37308 Heilbad Heiligenstadt, Germany; Faculty of Mathematics and Natural Sciences, Technische Universität Ilmenau, 98694 Ilmenau, Germany;* orcid.org/0000 0002 9237 3482; Email: thi huong.nguyen@iba heiligenstadt.de

Author

Gurunath Apte − *Institute for Bioprocessing and Analytical Measurement Techniques (iba), 37308 Heilbad Heiligenstadt, Germany; Institute of Nanotechnology (INT) and Karlsruhe Nano Micro Facility (KNMFi), Karlsruhe Institute of Technology, 76131 Karlsruhe, Germany;* orcid.org/0000 0002 4391 2152

Author Contributions

G.A. developed the methodology, performed the experiments, analyzed the data, discussed the results, and wrote the original draft of the article. T. H.N. and M.H. developed the study concept, discussed the results, performed the supervision, administered the project, acquired the funding, and wrote the article. All authors have read and agreed to the final version of the article.

Notes

The authors declare no competing financial interest.

■ ACKNOWLEDGMENTS

T. H.N. and G.A. acknowledge the support of the Freistaat Thüringen (Thüringer Ministerium für Wirtschaft, Wissen schaft und Digitale Gesellschaft, TMWWDG, Germany). T. H.N. acknowledges the partial support of the German Research Foundation (DFG) within the projects (Nrs 269095734 and 469240103). This work was partly carried out with the support of the Karlsruhe Nano Micro Facility (KNMFi, http://www.knmf.kit.edu) and Helmholtz Research Infrastructure at the Karlsruhe Institute of Technology (KIT, http://www.kit.edu). M.H. acknowledges the additional support by the Helmholtz Association in the form of a Helmholtz ERC Recognition Award.

■ REFERENCES

(1) Michelson, A. D. *Platelets*, 3rd ed.; Walker, H.; Hall, W.; Hurst, J., Eds.; Butterworths, 2019.

(2) Shin, E. K.; Park, H.; Noh, J. Y.; Lim, K. M.; Chung, J. H. Platelet Shape Changes and Cytoskeleton Dynamics as Novel Therapeutic Targets for Anti Thrombotic Drugs. *Biomol. Ther.* **2017**, *25*, 223−230.

(3) Apte, G.; Börke, J.; Rothe, H.; Liefeith, K.; Nguyen, T. H. Modulation of Platelet Surface Activation: Current State and Future Perspectives. *ACS Appl. Bio Mater.* **2020**, *3*, 5574−5589.

(4) Shadden, S. C.; Hendabadi, S. Potential Fluid Mechanic Pathways of Platelet Activation. *Biomech. Model. Mechanobiol.* **2013**, *12*, 467−474.

(5) Flaumenhaft, R.; Sharda, A. The Life Cycle of Platelet Granules. *F1000Research* **2018**, *7*, No. 236.

(6) Sangkuhl, K.; Shuldiner, A. R.; Klein, T. E.; Altman, R. B. Platelet Aggregation Pathway. *Pharmacogenet. Genomics* **2011**, *21*, 516−521.

(7) Yun, S. H.; Sim, E. H.; Goh, R. Y.; Park, J. I.; Han, J. Y. Platelet Activation: The Mechanisms and Potential Biomarkers. *BioMed Res. Int.* **2016**, *2016*, 1−5.

(8) Holinstat, M.; Preininger, A. M.; Milne, S. B.; Hudson, W. J.; Brown, H. A.; Hamm, H. E. Irreversible Platelet Activation Requires Protease Activated Receptor 1 Mediated Signaling to Phosphatidyli nositol Phosphates. *Mol. Pharmacol.* **2009**, *76*, 301−313.

(9) Jaffer, I. H.; Fredenburgh, J. C.; Hirsh, J.; Weitz, J. I. Medical Device Induced Thrombosis: What Causes It and How Can We Prevent It? *J. Thromb. Haemostasis* **2015**, *13*, S72−S81.

(10) Vit, G.; Klüter, H.; Wuchter, P. Platelet Storage and Functional Integrity. *J. Lab. Med.* **2020**, *44*, 285−293.

(11) Levy, J. H.; Neal, M. D.; Herman, J. H. Bacterial Contamination of Platelets for Transfusion: Strategies for Prevention. *Crit. Care* **2018**, *22*, No. 271.

(12) Al Salloum, H.; Saunier, J.; Dazzi, A.; Vigneron, J.; Etcheberry, A.; Marlière, C.; Aymes Chodur, C.; Herry, J. M.; Bernard, M.; Jubeli, E.; Yagoubi, N. Characterization of the Surface Physico Chemistry of Plasticized PVC Used in Blood Bag and Infusion Tubing. *Mater. Sci. Eng., C* **2017**, *75*, 317−334.

(13) Farrugia, B. L.; Chandrasekar, K.; Johnson, L.; Whitelock, J. M.; Marks, D. C.; Irving, D. O.; Lord, M. S. Perspectives on the Use of Biomaterials to Store Platelets for Transfusion. *Biointerphases* **2016**, *11*, No. 029701.

(14) Ventre, M.; Natale, C. F.; Rianna, C.; Netti, P. A. Topographic Cell Instructive Patterns to Control Cell Adhesion, Polarization and Migration. *J. R. Soc., Interface* **2014**, *11*, No. 20140687.

(15) Koh, L. B.; Rodriguez, I.; Venkatraman, S. S. The Effect of Topography of Polymer Surfaces on Platelet Adhesion. *Biomaterials* **2010**, *31*, 1533−1545.

(16) Ding, Y.; Leng, Y.; Huang, N.; Yang, P.; Lu, X.; Ge, X.; Ren, F.; Wang, K.; Lei, L.; Guo, X. Effects of Microtopographic Patterns on Platelet Adhesion and Activation on Titanium Oxide Surfaces. *J. Biomed. Mater. Res., Part A* **2013**, *101A*, 622−632.

(17) Bui, V. C.; Medvedev, N.; Apte, G.; Chen, L. Y.; Denker, C.; Greinacher, A.; Nguyen, T. H. Response of Human Blood Platelets on Nanoscale Groove Patterns: Implications for Platelet Storage. *ACS Appl. Nano Mater.* **2020**, *3*, 6996−7004.

(18) Lenhert, S.; Sesma, A.; Hirtz, M.; Chi, L.; Fuchs, H.; Wiesmann, H. P.; Osbourn, A. E.; Moerschbacher, B. M. Capillary Induced Contact Guidance. *Langmuir* **2007**, *23*, 10216−10223.

(19) Emmert, M.; Somorowsky, F.; Ebert, J.; Görick, D.; Heyn, A.; Rosenberger, E.; Wahl, M.; Heinrich, D. Modulation of Mammalian Cell Behavior by Nanoporous Glass. *Adv. Biol.* **2021**, *5*, No. 2000570.

(20) Wang, K.; Bruce, A.; Mezan, R.; Kadiyala, A.; Wang, L.; Dawson, J.; Rojanasakul, Y.; Yang, Y. Nanotopographical Modulation of Cell Function through Nuclear Deformation. *ACS Appl. Mater. Interfaces* **2016**, *8*, 5082−5092.

(21) Milner, K. R.; Snyder, A. J.; Siedlecki, C. A. Sub Micron Texturing for Reducing Platelet Adhesion to Polyurethane Bio materials. *J. Biomed. Mater. Res., Part A* **2006**, *76A*, 561−570.

(22) Mao, C.; Liang, C.; Luo, W.; Bao, J.; Shen, J.; Hou, X.; Zhao, W. Preparation of Lotus Leaf like Polystyrene Micro and Nanostruc ture Films and Its Blood Compatibility. *J. Mater. Chem.* **2009**, *19*, 9025−9029.

(23) Kita, A.; Sakurai, Y.; Myers, D. R.; Rounsevell, R.; Huang, J. N.; Seok, T. J.; Yu, K.; Wu, M. C.; Fletcher, D. A.; Lam, W. A. Microenvironmental Geometry Guides Platelet Adhesion and Spread ing: A Quantitative Analysis at the Single Cell Level. *PLoS One* **2011**, *6*, No. e26437.

(24) Pham, T. T.; Wiedemeier, S.; Maenz, S.; Gastrock, G.; Settmacher, U.; Jandt, K. D.; Zanow, J.; Lüdecke, C.; Bossert, J. Hemodynamic Aspects of Reduced Platelet Adhesion on Bioinspired Microstructured Surfaces. *Colloids Surf., B* **2016**, *145*, 502−509.

(25) Nandakumar, D.; Bendavid, A.; Martin, P. J.; Harris, K. D.; Ruys, A. J.; Lord, M. S. Fabrication of Semiordered Nanopatterned Diamond like Carbon and Titania Films for Blood Contacting Applications. *ACS Appl. Mater. Interfaces* **2016**, *8*, 6802−6810.

(26) Hulander, M.; Lundgren, A.; Faxälv, L.; Lindahl, T. L.; Palmquist, A.; Berglin, M.; Elwing, H. Gradients in Surface Nanotopography Used to Study Platelet Adhesion and Activation. *Colloids Surf., B* **2013**, *110*, 261−269.

(27) Qiu, Y.; Brown, A. C.; Myers, D. R.; Sakurai, Y.; Mannino, R. G.; Tran, R.; Ahn, B.; Hardy, E. T.; Kee, M. F.; Kumar, S.; Bao, G.; Barker, T. H.; Lam, W. A. Platelet Mechanosensing of Substrate Stiffness during Clot Formation Mediates Adhesion, Spreading, and Activation. *Proc. Natl. Acad. Sci. U.S.A.* **2014**, *111*, 14430−14435.

(28) Kee, M. F.; Myers, D. R.; Sakurai, Y.; Lam, W. A.; Qiu, Y. Platelet Mechanosensing of Collagen Matrices. *PLoS One* **2015**, *10*, No. e0126624.

(29) Apte, G.; Lindenbauer, A.; Schemberg, J.; Rothe, H.; Nguyen, T. H. Controlling Surface Induced Platelet Activation by Agarose and Gelatin Based Hydrogel Films. *ACS Omega* **2021**, *6*, 10963−10974.
(30) Zambelli, T.; Aebersold, M. J.; Behr, P.; Han, H.; Hirt, L.; Martinez, V.; Guillaume Gentil, O.; Vörös, J. FluidFM: Development of the Instrument as Well as Its Applications for 2D and 3D Lithography. In *Open Space Microfluidics: Concepts, Implementations, Applications*; John Wiley & Sons, 2018; pp 295−323.
(31) de Souza, J. V.; Liu, Y.; Wang, S.; Dörig, P.; Kuhl, T. L.; Frommer, J.; Liu, G. Y. Three Dimensional Nanoprinting via Direct Delivery. *J. Phys. Chem. B* **2018**, *122*, 956−962.
(32) Hirt, L.; Ihle, S.; Pan, Z.; Dorwling Carter, L.; Reiser, A.; Wheeler, J. M.; Spolenak, R.; Vörös, J.; Zambelli, T. Template Free 3D Microprinting of Metals Using a Force Controlled Nanopipette for Layer by Layer Electrodeposition. *Adv. Mater.* **2016**, *28*, 2311−2315.
(33) Berganza, E.; Hirtz, M. Direct Write Patterning of Biomimetic Lipid Membranes in Situ with FluidFM. *ACS Appl. Mater. Interfaces* **2021**, *13*, 50774−50784.
(34) LOCTITE AA 3491 Light cure, acrylic based instant adhesive Henkel Adhesives. https://www.henkel adhesives.com/de/en/product/uv curing adhesives/loctite aa 3491.html, (accessed March 22, 2022).
(35) Hertz, H. Ueber Die Berührung Fester Elastischer Körper. *crll* **1882**, *1882*, 156−171.
(36) Paddock, S. Confocal Reflection Microscopy: The "Other" Confocal Mode. *Biotechniques* **2002**, *32*, 274−276.
(37) Schneider, C. A.; Rasband, W. S.; Eliceiri, K. W. NIH Image to ImageJ: 25 Years of Image Analysis. *Nat. Methods* **2012**, *9*, 671−675.
(38) Abràmoff, M. D.; Magalhães, P. J.; Ram, S. J. Image Processing with ImageJ. In *Biophotonics International*; Laurin Publishing, 2004; Vol. *11*, pp 36−42.
(39) Hansen, C. E.; Qiu, Y.; McCarty, O. J. T.; Lam, W. A. Platelet Mechanotransduction. *Annu. Rev. Biomed. Eng.* **2018**, *20*, 253−275.
(40) Ruggeri, Z. M.; Mendolicchio, G. L. Adhesion Mechanisms in Platelet Function. *Circ. Res.* **2007**, *100*, 1673−1685.
(41) Xu, L. C.; Bauer, J. W.; Siedlecki, C. A. Proteins, Platelets, and Blood Coagulation at Biomaterial Interfaces. *Colloids Surf., B* **2014**, *124*, 49−68.
(42) Elbert, D. L.; Hubbell, J. A. Surface Treatments of Polymers for Biocompatibility. *Annu. Rev. Mater. Sci.* **1996**, *26*, 365−394.
(43) Majhy, B.; Priyadarshini, P.; Sen, A. K. Effect of Surface Energy and Roughness on Cell Adhesion and Growth Facile Surface Modification for Enhanced Cell Culture. *RSC Adv.* **2021**, *11*, 15467−15476.
(44) Firkowska Boden, I.; Helbing, C.; Dauben, T. J.; Pieper, M.; Jandt, K. D. How Nanotopography Induced Conformational Changes of Fibrinogen Affect Platelet Adhesion and Activation. *Langmuir* **2020**, *36*, 11573−11580.
(45) Berganza, E.; Apte, G.; Vasantham, S. K.; Nguyen, T. H.; Hirtz, M. Integration of Biofunctional Molecules into 3D Printed Polymeric Micro /Nanostructures. *Polymers* **2022**, *14*, No. 1327.
(46) Sugimoto, A.; Ohnoki, S.; Yamaguchi, H.; Okubo, Y. Oxygen Permeability of the Container Necessary for Storage of Platelet Concentrate. *J. Jpn. Soc. Blood Transfus.* **1989**, *35*, 26−31.
(47) Freedman, J. E. Oxidative Stress and Platelets. *Arterioscler., Thromb., Vasc. Biol.* **2008**, *28*, s11−s16.
(48) Potthoff, E.; Guillaume Gentil, O.; Ossola, D.; Polesel Maris, J.; LeibundGut Landmann, S.; Zambelli, T.; Vorholt, J. A. Rapid and Serial Quantification of Adhesion Forces of Yeast and Mammalian Cells. *PLoS One* **2012**, *7*, No. e52712.